Iranian Society of Acoustics and Vibration
The 15th ISAV2025 International Conference on Acoustics and Vibration
24-25 Dec 2025 Tehran- Iran

A Framework for Stress Detection and Fault Zone Characterization Using Optical Distributed Acoustic Sensing (DAS) Data

Sogol Aslan Sefat[a], Aghil Yousefi Koma[b*], Mohammad Yousof Dehghan[c], Mohammad Amin Azari[d]

[a] *Member of Center of Advanced Systems and Technologies (CAST), School of Mechanical Engineering, Tehran University, 1417466191, Tehran, Iran.*

[b*] *Head of Center of Advanced Systems and Technologies (CAST), School of Mechanical Engineering, Tehran University, 1417466191, Tehran, Iran.*

[c] *Member of Center of Advanced Systems and Technologies (CAST), School of Mechanical Engineering, Tehran University, 1417466191, Tehran, Iran.*

[d] *Member of Center of Advanced Systems and Technologies (CAST), School of Mechanical Engineering, Tehran University, 1417466191, Tehran, Iran.*

* *Corresponding author e-mail: aykoma@ut.ac.ir*

Abstract

This study presents a practical workflow for extracting and analyzing stress from Distributed Acoustic Sensing (DAS) measurements. The main contribution is the direct use of DAS signals to obtain quantitative, localized stress estimates and to evaluate how human activities—specifically construction and traffic—affect faults, an application that has received limited attention in prior DAS-based studies. Raw DAS data (Rayleigh backscattered intensity) are first preprocessed to remove noise and long-term trends. The signals are then demodulated using Hilbert-based analysis to obtain an unwrapped, unambiguous phase and to estimate phase changes. After converting phase variations to strain (or strain rate), stress is computed using the shear modulus of the optical fiber. Results indicate that stress perturbations induced by construction and traffic are clearly distinguishable and measurable, and that their magnitudes vary with source distance and local geological conditions. The extracted stress patterns can be used to identify vulnerable fault segments and potential hazard zones, providing actionable information for geological risk assessment and urban planning. Overall, the proposed procedure offers strong potential for scalable, continuous DAS-based monitoring in diverse settings.

Keywords: Fiber-Optic Sensor; Distributed Acoustic Sensing (DAS); Stress Analysis; Fault Zone Monitoring.

1. Introduction

Distributed Acoustic Sensing (DAS) has recently proven to be an effective method for real-time and continuous monitoring of geophysical and engineering environments [2, 5, 9]. The method uses telecommunication optical fibers as strain sensors distributed over long distances. Recent improvements in DAS technology allow the observation of subtle signals generated in the subsurface due to either natural phenomena or artificial processes [1, 10].

In urban and infrastructure environments, construction works, heavy equipment, and vehicular traffic are some of the most likely producers of stress perturbations that might affect geological structures surrounding faults [4]. It becomes essential to understand stress patterns in these environments and how these might interact with geological conditions [5, 9]. Though past approaches mostly concentrated on seismic imaging and vibration detection with DAS [2, 6], there are comparatively less attempts to compute stress values due to environmental factors [7, 8]. In this paper, we attempt to build on this narrative with our novel method to obtain and analyze stress values through DAS measurements on various environmental data sets with application to the DAS data set presented by Tomasov et al. [1]. In that dataset, a standard single-mode ITU-T G.652.D fiber is buried ~1 m underground alongside the pavement and interrogated with an OptaSense ODH-F (Φ-OTDR) system, providing a representative urban deployment for event classification and stress analysis [1].

2. Research Background

In distributed acoustic sensing (DAS), the interference of Rayleigh-backscattered light from two closely spaced fiber segments is measured. Spatiotemporal variations in axial strain (and temperature) modulate the optical phase of the backscattered signal [2, 8]. Under standard small-signal assumptions, the measured differential phase over a gauge length $L_g$is, to first order, linearly related to the gauge-averaged axial strain $\bar{\varepsilon}$, with an additive temperature term:

$$\Delta\phi(t,z) = \frac{4\pi n_{\text{eff}}}{\lambda_0}\,\xi\,L_g\,\bar{\varepsilon}(t,z) + \frac{4\pi n_{\text{eff}}}{\lambda_0}\,L_g\,\kappa_T\,\Delta T(t,z). \tag{1}$$

Here, $\lambda_0$is the laser wavelength, $n_{\text{eff}}$the effective refractive index, $\xi \simeq 1 - p_e$(with $p_e$the effective photoelastic coefficient), and $\kappa_T$groups thermo-optic and thermal-expansion contributions. This linear phase–strain model (with an additive temperature term) is standard for Rayleigh-based DAS.

The gauge length $L_g$is set by interrogator timing and pulse shaping and can be viewed as the spatial separation of the two backscattering sub-segments whose interference is demodulated. Practical systems often use optical pulse widths smaller than, and on the order of, L_g, so the DAS response acts as a spatial average over L_g [3, 7].

Rearranging Eq. (1) (and neglecting temperature, or after temperature compensation), the gauge-averaged strain is:

$$\bar{\varepsilon}(t,z) = \frac{\lambda_0}{4\pi n_{\mathrm{eff}}\ \xi\ L_g}\ \Delta\phi(t,z) \tag{2}$$

This is the explicit form of Eq. (1) used here.
For phase demodulation with intensity-only ϕ-OTDR traces $I(t,z)$, form the analytic signal via the Hilbert transform $H\{\cdot\}$:

$$a(t,z) = I(t,z) + j\,H\{I(t,z)\} \tag{3a}$$
$$\phi(t,z) = \arg\ a(t,z) \tag{3b}$$

The phase change relative to a temporal reference $t_0$is

$$\Delta\phi(t,z) = \phi(t,z) - \phi(t_0,z) \tag{4}$$

When coherent I/Q traces are available, the instantaneous phase is obtained directly as

$$\phi(t,z) = \arg\left(I(t,z) + j\,Q(t,z)\right) \tag{5}$$

Spatially differential demodulation may be performed by differencing adjacent channels; for channel spacing Δz,

$$\delta_z\phi(t,z_k)\ \approx\ \phi(t,z_{k+1}) - \phi(t,z_k) \tag{6}$$

which still corresponds to a gauge-average over the effective L_g.

Many energy and dynamical analyses use strain-rate, obtained as the time derivative of the unwrapped phase (optionally after band-limiting $\phi$to improve SNR):

$$\dot{\varepsilon}(t,z) = \frac{\lambda_0}{4\pi n_{\mathrm{eff}}\ \xi\ L_g}\ \frac{\partial}{\partial t}\,\Delta\phi(t,z) \tag{7}$$

This conversion from phase (or strain) to strain-rate is standard in DAS workflows.

In this study we use an OptaSense ODH-F (ϕ-OTDR) interrogator with the following acquisition parameters: laser wavelength $\lambda_0 = 1550\ nm$; pulse width $= 20\ ns$; pulse-repetition rate / temporal sampling $= 20\ kHz$; gauge length $L_g = 1.02\ m$; number of channels $= 1663$ fiber type ITU-T G.652.D; and data format HDF5 with event labels [1].

After estimating axial strain, the corresponding axial stress in the linear elastic regime should be computed using Young's modulus E for uniaxial loading [3, 6]:

$$\sigma = E\ \varepsilon(\text{uniaxial}) \tag{8}$$

Shear stress relates to shear strain via

$$\tau = G\,\gamma \tag{9}$$

The elastic constants satisfy

$$E = 2G(1+\nu) \tag{10}$$

with Poisson's ratio ν. For standard silica fibers at room temperature, representative values are $E \simeq 66\text{–}75$, $G \simeq 28\text{–}32$ GP, and $\nu \simeq 0.15\text{–}0.19$ [3, 8]. Use the modulus appropriate to the material bearing the load, and the correct constitutive form for plane-stress/plane-strain if applicable.

If temperature variations are significant within the analysis band, compensate using an independent temperature estimate (e.g., DTS) or a joint model, since both thermo-optic and thermal-expansion terms also modulate $\Delta\phi$in Eq. (1). These considerations ensure that the mapping from phase to strain (and strain-rate), and then to stress, is performed with the accuracy and stability required for DAS-based analyses [4, 5, 9].

3. Methodology

The proposed methodology consists of three main stages: (1) data preprocessing, (2) phase demodulation and stress estimation, and (3) spatial–temporal analysis of stress patterns. Each stage is designed to ensure reproducibility, noise robustness, and physical interpretability of the DAS measurements [1, 7].

3.1 Data Acquisition and Preprocessing

Raw DAS data, recorded as Rayleigh backscattering intensity, were collected along optical fibers deployed across target areas influenced by construction activities and vehicle movement. The raw amplitude traces were first detrended and bandpass-filtered to remove environmental and system-related noise [1, 6].

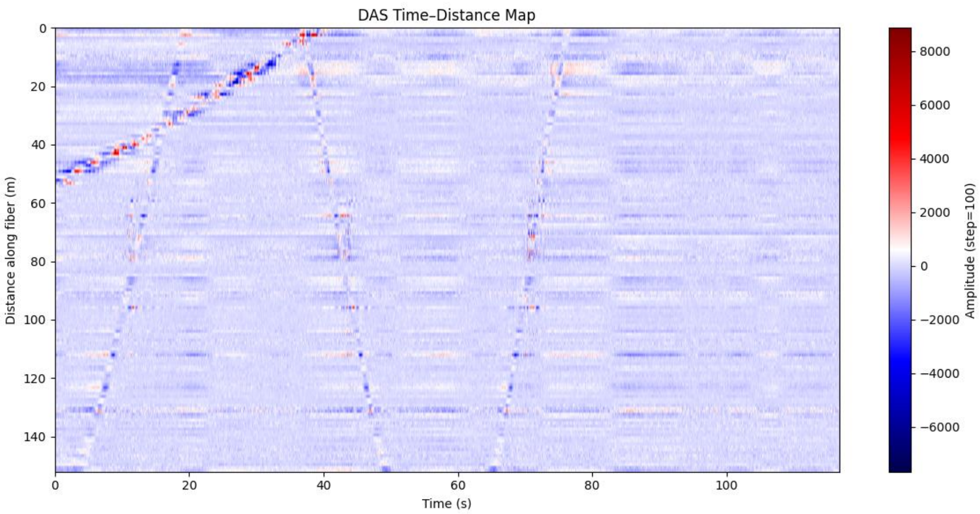

Figure 1. DAS time-distance map for car dataset.

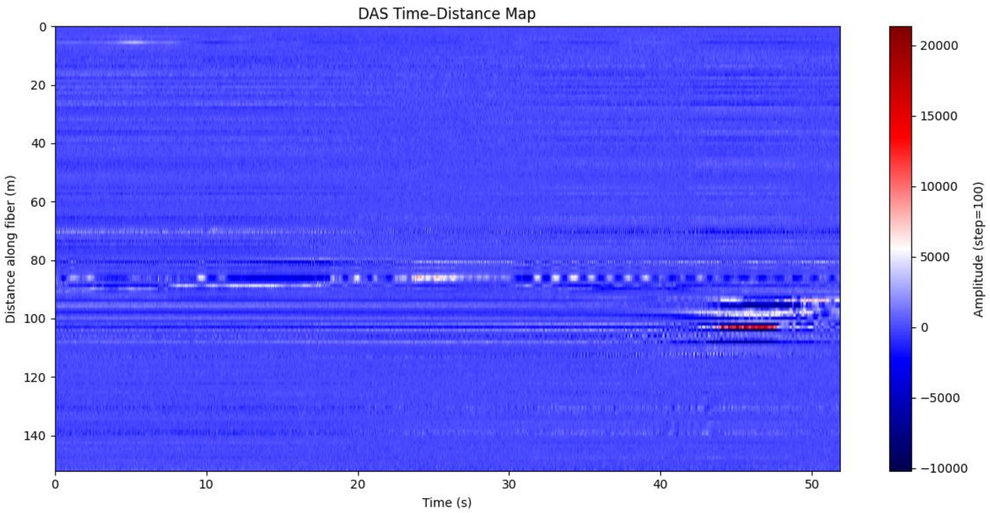

Figure 2. DAS time-distance map for construction dataset.

3.2 Phase Extraction and Conversion to Stress

After preprocessing, the analytic signal was computed using the Hilbert transform, and the unwrapped phase was extracted [2, 7]. The phase difference relative to a reference time frame was then converted to strain according to Equation (2) [3]. In this stage, baseline stability and phase recovery were also qualitatively verified to ensure effective removal of low-frequency noise and instrument-related jumps, enabling reliable linear elastic scaling from strain to stress.

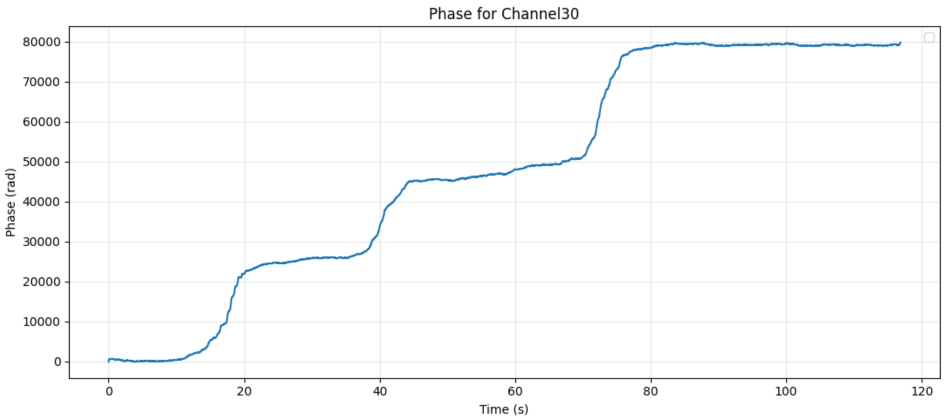

Figure 3. unwrapped phase time series for the car dataset, channel 30 shown as an example.

The unwrapped phase in channel 30 evolves smoothly with intermittent step-like excursions; the discrete, slanted segments correspond to vehicles passing the sensing point, while quiet intervals relax back toward a stable baseline, indicating successful preprocessing and robust Hilbert-based phase retrieval.

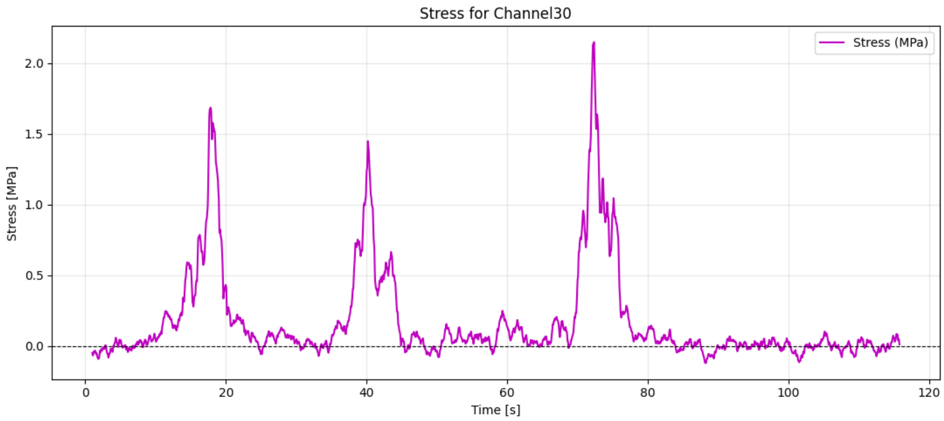

Figure 4. Stress time series for the car dataset, channel 30 shown as an example.

Converting the same record to stress reveals short-lived spikes about a near-zero baseline whose amplitudes and durations track individual transits.

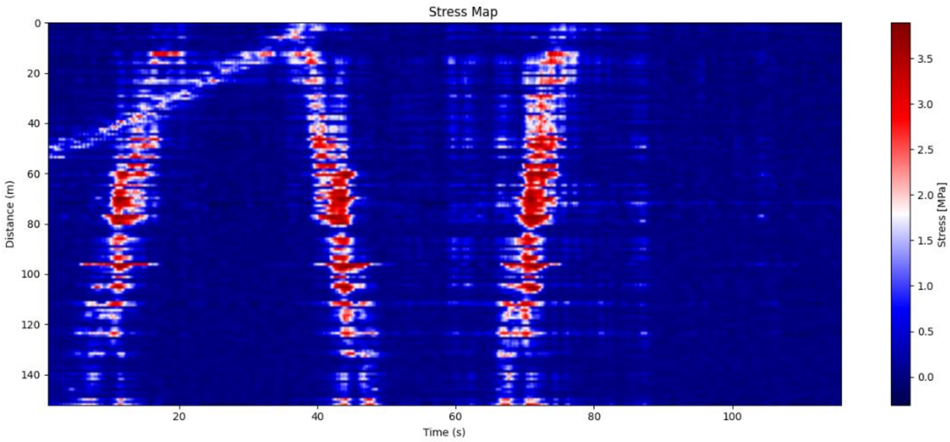

Figure 5. Strain time-distance map for the car dataset.

The strain time–distance map displays clear oblique streaks whose slopes reflect apparent source velocities and whose lateral continuity indicates coherent moving fronts that persist across multiple channels.

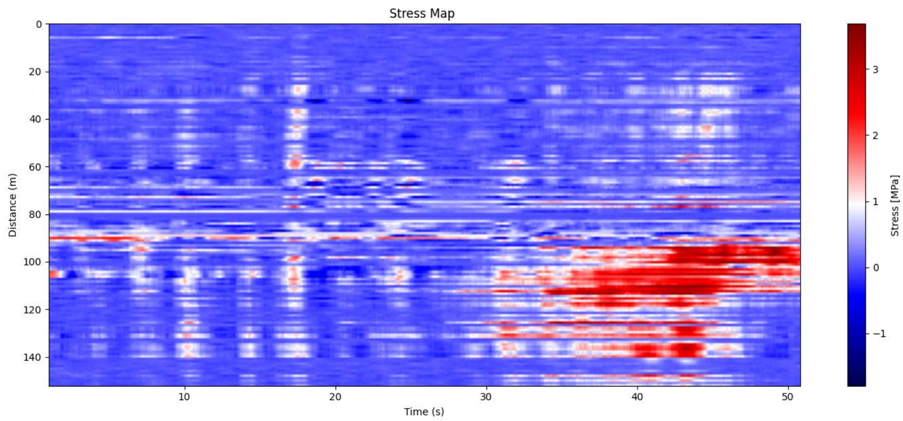

Figure 6. Strain time-distance map for the construction dataset.

By contrast, the construction dataset is dominated by predominantly vertical, spatially confined streaks, diagnosing a largely stationary source that imposes sustained loading near a fixed position.

3.3 Stress Pattern Analysis and Fault Response Evaluation

Based on the time–distance maps (Figures 5 and 6), the vehicle dataset can be interpreted as showing oblique streaks and moving fronts, whereas the construction dataset appears to contain predominantly vertical, spatially confined streaks that are consistent with more stationary loading [9, 10]. Within the Stress Pattern Analysis and Fault Response framework, and assuming elastic behavior, the applied shear strain γ in a damage zone would be expected to relate approximately linearly to shear stress τ ($\tau \approx G\gamma$); accordingly, meaningful comparisons of amplitude and duration should rely on a stress scale that is calibrated to local material properties and coupling conditions [4]. The reference study for an intact-sandstone damage zone with Young's modulus E ≈ 15 GPa suggests a shear strength on the order of ~7–17 MPa, which may serve as a tentative benchmark for proximity to failure under comparable conditions [4].

Under these working assumptions and the present calibration, the peak stresses inferred for the vehicle group (≈4 MPa) lie below that benchmark and are indicative of relatively short-lived, localized perturbations [5]. The brevity of these peaks likely limits effective loading time, with the system tending to relax toward baseline after each passage. For the construction group, the corresponding peak value (≈3.5 MPa) also remains below the cited range but appears to persist for longer durations, which could keep τ nearer upper bounds for extended intervals and, in some scenarios, imply a comparatively higher mechanical concern [9, 10]. Even if sub-threshold, such persistence might contribute to incremental inelastic effects (e.g., microcrack growth) and a heightened susceptibility under additional perturbations or environmental changes [4]. As summarized in Table 1, both anthropogenic datasets are interpreted to fall below the geodetically inferred strength range (7–17 MPa) for the referenced setting, while differing in loading duration and apparent recovery behavior; these interpretations remain contingent on site-specific properties and calibration choices.

Table 1. Quantitative comparison of stress and fault-response characteristics

Parameter	Vehicle Dataset	Construction Dataset	Fault Damage Zone (Li et al., 2024)
Maximum stress (τ_{max})	~4.0 MPa	~3.5 MPa	7–17 MPa
Mean loading duration	1–5 s	10–25 s	Continuous (tectonic)
Shear strain (γ_{max})	$\sim 6.0\times10^{-4}$	$\sim 6.0\times10^{-4}$	$8\times10^{-4} - 2\times10^{-3}$
Shear modulus (G)	5.8 GPa	5.8 GPa	4–8 GPa

4. Conclusion

The proposed framework provides a practical and reliable approach for stress extraction and analysis from Distributed Acoustic Sensing (DAS) data [1, 2, 6]. By employing analytic phase demodulation and systematic mapping from Rayleigh backscattering intensity to strain and stress, the method enables accurate identification of stress patterns induced by anthropogenic activities such as vehicle movement and construction operations [9]. The results indicate that the nature and persistence of loading play a key role in influencing local fault susceptibility [4, 5].

Overall, the developed framework offers a robust tool for continuous subsurface monitoring, hazard assessment, and engineering–urban decision-making [7, 9, 10]. Its adaptability to other natural and anthropogenic contexts suggests promising potential for integration into intelligent seismic and geotechnical monitoring systems at urban and regional scales [5, 8, 9].

REFERENCES

1. A. Tomasov, P. Zaviska, P. Dejdar, O. Klicnik, T. Horvath and P. Munster, "Comprehensive Dataset for Event Classification Using Distributed Acoustic Sensing (DAS) Systems", *Scientific Data* 12, 793 (2025).
2. A. Xenaki, P. Gerstoft, E. Williams and S. Abadi, "Overview of Distributed Acoustic Sensing: Theory and Ocean Applications", *Journal of the Acoustical Society of America* 158(1), 801–825 (2025).
3. I. Alj, M. Quiertant, A. Khadour, Q. Grando, B. Terrade, J.-C. Renaud and K. Benzarti, "Experimental and Numerical Investigation on the Strain Response of Distributed Optical Fiber Sensors Bonded to Concrete: Influence of the Adhesive Stiffness on Crack Monitoring Performance", *Sensors (Basel)* 20(18), 5144 (2020).
4. C. Li, Z. Ma, X. Xi, G. Zhang and X. Shan, "Constraining Shear Strength of Fault Damage Zone Using Geodetic Data and Numerical Simulation", *Geophysical Research Letters* 51, e2024GL108169 (2024).
5. Lior, I., Zhan, Z., Lindsey, N. J., and Ajo-Franklin, J. B., "Strain to Ground Motion Conversion of Distributed Acoustic Sensing Data for Earthquake Magnitude and Stress Drop Determination", *Solid Earth* 12, 1421–1436 (2021).
6. Sherman, D., "Geomechanical Modeling of Distributed Fiber-Optic Sensor Arrays", *The Leading Edge* 38(6), 458–466 (2019).
7. Forbriger, T., Walter, F., Sollberger, D., and Lindsey, N., "Calibration of the Strain Amplitude Recorded with DAS Using a Strainmeter Array", *arXiv preprint* arXiv:2408.01151 (2024).
8. Jiang, X., Zhang, Y., Chen, L., et al., "How the Material Characteristics of Optical Fibers and Soil Conditions Affect Distributed-Acoustic Sensing Measurements", *Sensors* 23(15), 6572 (2023).
9. Li, P., Xu, Z., Wang, D., and Sun, H., "Quantifying the Surface Strain Field Induced by Active Sources with Distributed Acoustic Sensing", *Sensors* 22(12), 4589 (2022).
10. Zhang, T., Li, Y., and Chen, Q., "Understanding Strain Signals from Low-Frequency Distributed Acoustic Sensing In-Well Measurements", *Society of Petroleum Engineers Journal* 29(11), 5896–5912 (2023).